

Correlating structure with fluorescence emission in phase-separated conjugated-polymer blends

JOHN CHAPPELL¹, DAVID G. LIDZEY*¹, PAUL C. JUKES¹, ANTHONY M. HIGGINS¹, RICHARD L. THOMPSON², STEPHEN O'CONNOR³, ILARIA GRIZZI³, ROBERT FLETCHER⁴, JIM O'BRIEN⁴, MARK GEOGHEGAN¹ AND RICHARD A. L. JONES¹

¹Department of Physics and Astronomy, The University of Sheffield, Hicks Building, Hounsfield Road, Sheffield S3 7RH, UK

²Department of Chemistry, University of Durham, South Road, Durham DH1 3LE, UK

³Cambridge Display Technology Ltd, Greenwich House, Madingley Rise, Madingley Road, Cambridge CB3 0HJ, UK

⁴The Dow Chemical Company Ltd, Building 1702, Midland, Michigan 48674, USA

* e-mail: d.g.lidzey@sheffield.ac.uk

Published online: 17 August 2003; doi:10.1038/nmat959

Blends of conjugated polymers are frequently used as the active semiconducting layer in light-emitting diodes and photovoltaic devices. Here we report the use of scanning near-field optical microscopy, scanning force microscopy and nuclear-reaction analysis to study the structure of a thin film of a phase-separated blend of two conjugated polymers prepared by spin-casting. We show that in addition to the well-known micrometre-scale phase-separated morphology of the blend, one of the polymers preferentially wets the surface and forms a 10-nm-thick, partially crystallized wetting layer. Using near-field microscopy we identify unexpected changes in the fluorescence emission from the blend that occurs in a 300-nm-wide band located at the interface between the different phase-separated domains. Our measurements provide an insight into the complex structure of phase-separated conjugated-polymer thin films. Characterizing and controlling the properties of the interfaces in such films will be critical in the further development of efficient optoelectronic devices.

Blending conjugated polymers with different electronic functionalities is an attractive method to create new materials for use in light-emitting diodes^{1–4} (LEDs) and photovoltaic devices^{5–8} (PVs). Such an approach is often necessary because most conjugated polymers have a much larger mobility for holes than they have for electrons. By blending hole-transporting and electron-transporting polymers together, thin films can be created (by, for example, spin-coating) in which the mobility (and thus transport) of both types of carriers is more balanced⁹. In LEDs, this technique has been used to maximize the electroluminescence efficiency⁶. It is well known, however, that blends of dissimilar polymers often undergo phase separation when cast into a thin film from solution due to the low entropy of mixing between different polymers¹⁰. Such strong phase separation is often exploited in polymer-blend PVs, because exciton dissociation into pairs of oppositely charged polarons can be promoted at an interface between the phase-separated components¹¹. In many practical devices, excitons are photogenerated at some distance from an interface. For exciton dissociation to compete with normal spontaneous emission, excitons must diffuse to such an interface within their lifetime. Because the exciton diffusion distance in conjugated polymers is rather small (≤ 10 nm)^{12,13}, it is important to have a large interfacial area within the active organic layer because this maximizes charge-carrier generation efficiency. The bicontinuous structures that are often found in phase-separated films can also provide efficient routes for charge carriers to be extracted from a PV device without subsequent recombination¹⁴.

Although the optimization of polymer-blend LED and PV performance can in principle be made without recourse to evaluating the microscopic structure of the film, there is a clear need to identify the mechanisms by which the properties of the blend influence the performance and efficiency of the device. The structure of thin films of phase-separated polymer blends prepared by spin-coating arises

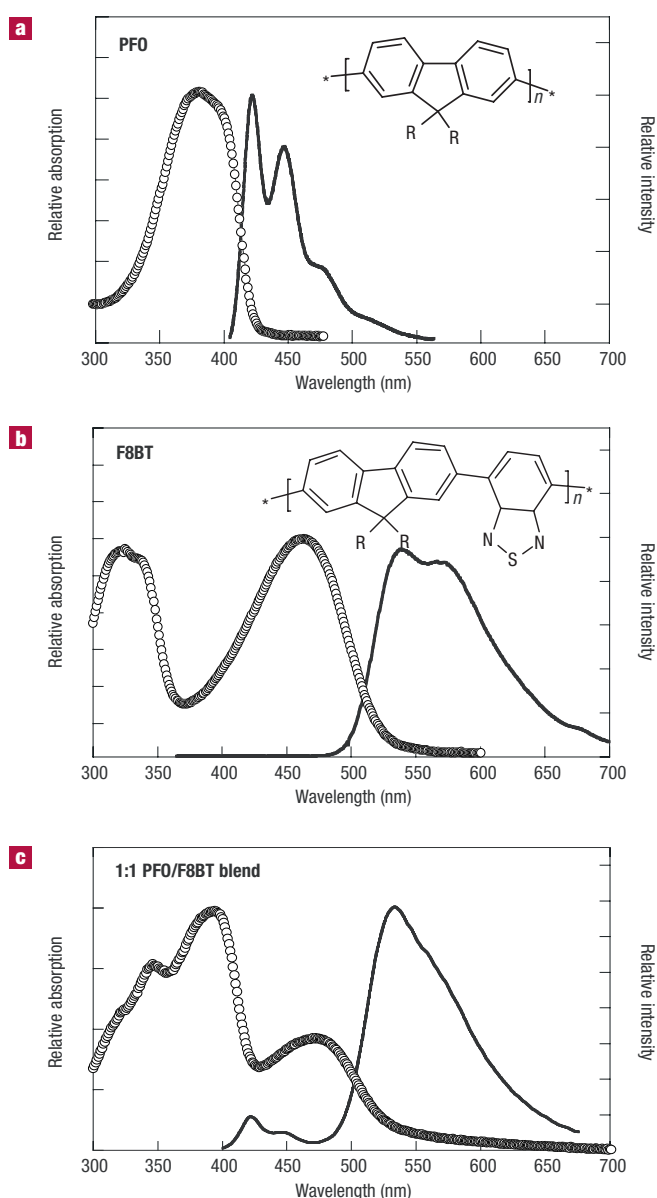


Figure 1 The absorption and fluorescence of PFO, F8BT and a (1:1) blend of PFO and F8BT. **a**, Absorption (circles) and photoluminescence emission (solid line) of poly(9,9'-dioctylfluorene) (PFO). **b**, Absorption (circles) and photoluminescence emission (solid line) of poly(9,9'-dioctylfluorene-*alt*-benzothiadiazole) (F8BT). The chemical structure of PFO and F8BT are shown as insets (where R = C₈H₁₇). **c**, Absorbance and fluorescence (following far-field excitation at 362 nm) of a 1:1 blend film of PFO and F8BT.

from a complex competition between several non-equilibrium processes, such as solvent evaporation, phase separation and subsequent phase coarsening, and possibly local ordering. Even for well-characterized 'classical' polymers, our understanding of the origins of thin-film morphology is incomplete¹⁰, so for conjugated polymers, for which basic physical properties are only imperfectly characterized, the task is all the more challenging.

In this paper, we report our use of a combination of techniques to characterize a blend of the conjugated polymers poly(9,9'-dioctylfluorene) (PFO) and poly(9,9'-dioctylfluorene-*alt*-benzothiadiazole) (F8BT). Blends of PFO and F8BT have been

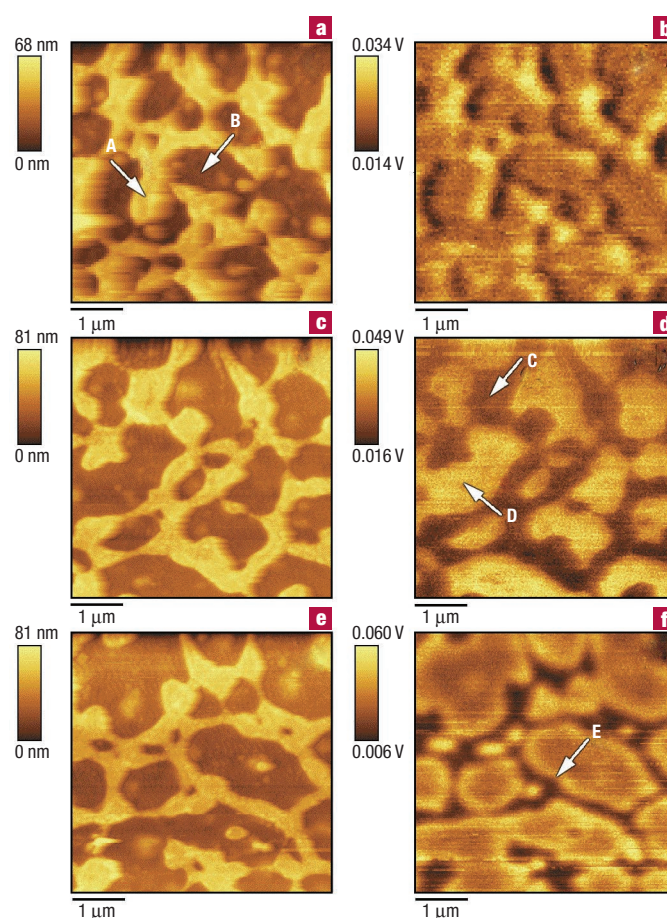


Figure 2 Scanning near-field optical micrographs of the transmission and fluorescence from a PFO/F8BT blend. **a, b**, The topography of a (1:1) PFO/F8BT blend (**a**) and the ultraviolet transmission of the film collected simultaneously (**b**). Arrow A indicates an F8BT-rich domain, and arrow B a PFO-rich domain. **c, d**, The film topography taken from a different point (**c**), and its respective F8BT fluorescence (**d**). Arrow C indicates an F8BT-rich domain, and arrow D a PFO-rich domain. **e, f**, The film topography from another point (**e**) and its respective PFO fluorescence (**f**). Arrow E indicates the brighter PFO emission that is observed at the PFO/F8BT boundary.

successfully used in LEDs^{3,4}, with blends of 95% PFO and 5% F8BT having optimal performance in devices. F8BT has also been used widely in polyfluorene-blend PV devices^{8,11,14–16}. The chemical structures, absorption and fluorescence of PFO and F8BT are shown in Fig. 1a and b respectively. PFO emits blue fluorescence following ultraviolet excitation with a quantum efficiency¹⁷ exceeding 50%. It also has a high hole-mobility¹⁸. F8BT emits green fluorescence with a quantum yield of ~50% following excitation using blue light¹⁹. F8BT has been shown to block hole transport and has a large but dispersive electron mobility²⁰. Time-resolved spectroscopic measurements show that excitons photogenerated on PFO molecules can rapidly transfer to F8BT molecules over distances of ~5 nm by Förster transfer (dipole–dipole coupling)²¹.

To characterize the micro- and nanostructure of the polymer blend, we have used a range of surface and bulk-sensitive techniques, each of which provides a complementary set of structural information. To characterize surface topography we have used scanning force microscopy (SFM). Although SFM provides a

high-resolution image of the surface structure, it cannot easily provide information regarding the local chemical composition. We have thus used scanning near-field optical microscopy (SNOM or NSOM) to map the local fluorescence emission from the blend. SNOM is a powerful technique that allows the optical properties of a surface to be resolved at length scales that are significantly shorter than the classical diffraction limit. It also has additional advantages over conventional fluorescence microscopy, as the optical image is often accompanied by a simultaneous measurement of surface topography. SNOM has been used to map the relative distribution of polymers in a blend by selectively exciting fluorescence from one of the components^{22–28}. The fluorescence emission generated from a conjugated polymer thin film using a SNOM mainly comes from regions within ~ 30 nm of the film surface, due to the relatively large extinction coefficient of conjugated polymers. To characterize the blend composition normal to the surface, we have used ^3He nuclear-reaction analysis (NRA) to generate a cross-sectional profile of the blend composition with a depth resolution (near the film surface) of ~ 6.5 nm (full-width at half-maximum). By combining these three techniques on a blend of functional polymers, we are able to provide a detailed picture of both the micro- and nanostructure of the blend, and we demonstrate the complex nature of interfaces between different phase-separated domains.

Blends of F8BT and PFO have been previously studied using SNOM^{27,28}. In these initial studies, the excitation was made directly into the F8BT and it was shown that the film was composed of PFO- and F8BT-rich phases, with the PFO-rich phase containing some F8BT. In our SNOM imaging, the blend is excited at 362 nm—a wavelength close to the absorption maximum of PFO and an absorption minimum of F8BT. The consequence of this is that we are able to study the transfer of energy between the PFO and F8BT molecules in the blend, and correlate this relative efficiency of transfer with the film composition and morphology.

Figure 1c shows the (far-field) absorption and fluorescence emission of a 60-nm-thick film of a 1:1 blend of PFO/F8BT following excitation at 362 nm. The emission spectrum from this blend film is dominated by the F8BT fluorescence. This occurs due to the strong overlap of PFO fluorescence with F8BT absorption, which permits dipole–dipole coupling between the materials and thus energy transfer from PFO to F8BT. It can be seen, however, that there is a small component of PFO emission in the spectrum (visible around 425 nm). This residual PFO emission corresponds to approximately 5% of the total luminescence, indicating that Förster transfer from PFO to F8BT in 1:1 blends is incomplete. Such residual PFO emission has been previously observed from PFO/F8BT blends, and it has been shown that such emission can be promoted by contact of the blend film with acetone²⁹. As we show below, the incomplete energy transfer that we observe in the blend films is consistent with local demixing of PFO and F8BT.

We characterized the micrometre-scale morphology of these blend films using transmission-mode SNOM. A series of measurements were made either mapping the transmission of the ultraviolet laser light (at wavelength $\lambda = 362$ nm) through the sample, or selectively mapping either the (blue) PFO or (green) F8BT fluorescence. Figure 2a,b shows a 5×5 μm shear-force image of the film topography and ultraviolet transmission through the film, respectively. It can be seen that the film topography is characterized by two phases, one of which appears to be almost continuous (see arrow A). The raised structures that we observe have been identified²⁷ as being rich in F8BT. The surrounding phase (identified by arrow B) has been similarly identified as being rich in PFO. When comparing the ultraviolet transmission with the topography, we find that the intensity of the laser-light transmitted (I_T) through the raised continuous phase is (3.0 ± 1.0) times greater than that transmitted through the lower-lying phase. This increased transmission through the raised continuous phase is in agreement with its assignment as being

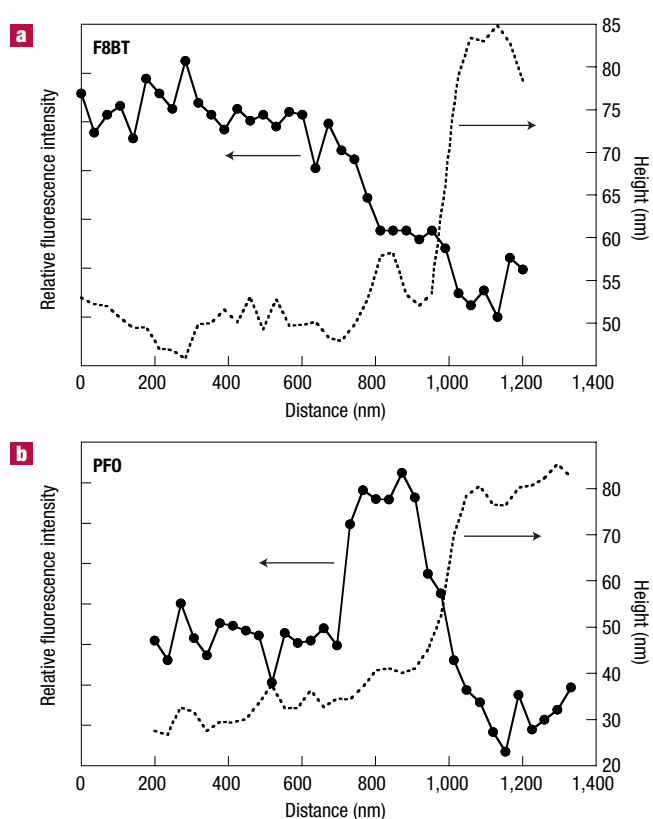


Figure 3 Fluorescence and topography cross-sections across an interface in a PFO/F8BT polymer blend. **a**, Topographic cross-section (dotted line) across a PFO/F8BT boundary. The F8BT domain protrudes by approximately 35 nm above the surface of the PFO-rich domain. The intensity of the F8BT fluorescence measured across the boundary is also shown using filled-circles. **b**, Topographic cross-section (dotted line) across a PFO/F8BT boundary. The PFO emission measured across the same boundary is shown using filled-circles.

F8BT-rich. Note that the low transmission observed at the right-hand edge of each of the F8BT-rich domains is an artefact, probably resulting from the SNOM probe being held at a slight angle with respect to the plane of the film.

When the transmitted laser signal is compared with the intensity of the incident laser (I_0), we estimate (neglecting reflection) the relative absorption in the film using $A = 1 - (I_T/I_0)$. We find the absorption in the PFO-rich phase $A_{\text{PFO}} = 0.85$, and the absorption in the F8BT-rich phase $A_{\text{F8BT}} = 0.40$. It thus appears that around twice as much light is absorbed in the PFO-rich phase compared with the F8BT-rich phase. From far-field absorption measurements we find that the extinction coefficient at the laser wavelength of PFO is approximately nine times larger than that of F8BT ($\alpha_{362\text{ nm}}^{\text{PFO}} = 3.60 \times 10^5 \text{ cm}^{-1}$ and $\alpha_{362\text{ nm}}^{\text{F8BT}} = 4.2 \times 10^4 \text{ cm}^{-1}$). This suggests that there is a significant fraction of both PFO and F8BT present within each of the two phases.

More information on the composition of the two phases is obtained from SNOM images of the fluorescence emission from the blend film. Figure 2c,d shows the topography and F8BT emission, respectively. These measurements were made at a different point from those presented in Fig. 2a,b, however a very similar surface topography and fluorescence distribution is observed across the whole film surface. The F8BT fluorescence is highly structured and is approximately two times more intense from the PFO-rich regions (arrow D) compared

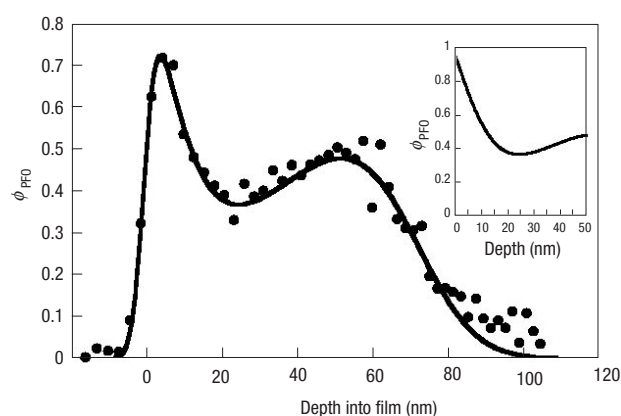


Figure 4 The d-PFO volume fraction (ϕ_{PFO}) depth profile of a 70-nm-thick film of a 1:1 d-PFO/F8BT blend as determined by nuclear-reaction analysis. In this technique, a beam of He ions accelerated to 700 KeV using a tandem accelerator³² is incident on a film that contains a deuterium-labelled component. The ${}^3\text{He}^{2+}$ undergoes the following nuclear reaction (${}^3\text{He}^{2+} + \text{d} \rightarrow ({}^4\text{Li}^{3+})^* \rightarrow \alpha + \text{p}$). The protons emitted from the film have a characteristic energy spectrum dependent on the energy of the reaction, which is also dependent on the depth in the film at which the reaction took place. By measuring the energy spectrum of the emitted protons, and knowing the angle from the film to the detector, the depth profile of the deuterium-labelled component within the film can be determined. The data points (filled circles) show the measured distribution of d-PFO as a function of depth from the film surface. The solid line is a best fit to the data. The inset shows the relative fraction of d-PFO in the near-surface region, extracted from the best-fit analysis (that is, excluding the effect of the finite experimental resolution). It can be seen that at the film surface, the d-PFO fraction approaches unity.

with that from the F8BT rich regions (arrow C). The high optical resolution that can be obtained using SNOM can be seen in Fig. 2d. From the sharpness of the edges of the F8BT fluorescence detected from the PFO-rich domains, we estimate the resolution of the SNOM image to be around 70 nm (equivalent to $\sim \lambda/8$).

The observation of F8BT emission from the PFO-rich phase is consistent with the PFO-rich phase containing some fraction of F8BT. We can quantitatively understand the difference in the intensity of F8BT emission from the PFO- and F8BT-rich domains on the basis of the relative absorption at the laser wavelength of the different phases; the ultraviolet-transmission SNOM measurements demonstrated that approximately twice as much light is absorbed in the PFO-rich phase compared with the F8BT-rich phase. Far-field photoluminescence spectra indicate that $\sim 90\%$ of excitons primarily photogenerated on PFO molecules subsequently transfer to F8BT molecules. If we assume the quantum yield for F8BT fluorescence is approximately the same in both phases, we should expect around twice as much F8BT emission from the PFO-rich phase compared with the F8BT-rich phase; a value in good agreement with our experimental observation.

Figure 2e,f shows the surface topography and PFO emission respectively, again measured at a different point on the film surface. Rather surprisingly, we observe residual PFO emission from the F8BT-rich phase, however this is around 3.5 times weaker than is observed from the centre of the PFO-rich phase. The most striking feature of the image is the fact that the PFO emission is brightest close to the boundary between the PFO- and F8BT-rich phases (arrow E). The PFO emission also appears more diffuse than the highly structured F8BT emission, particularly at the boundary between the PFO- and F8BT-rich phases. We compare the distribution of PFO and F8BT fluorescence in Fig. 3. Figure 3a compares a cross-section of the film

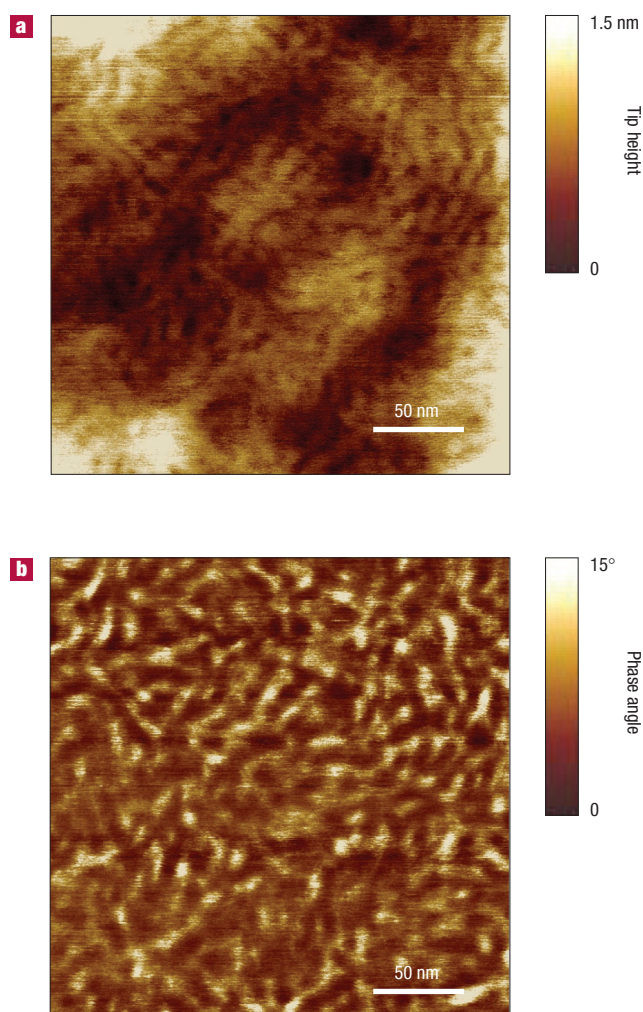


Figure 5 The structure of a PFO-rich domain as measured using a scanning force microscope. A Digital Instruments Nanoscope IIIa was used. **a**, Tapping-mode image recorded in the centre of a PFO-rich domain. **b**, The phase-contrast image associated with the topographic scan shown in **a**.

topography across a boundary between a PFO-rich and a F8BT-rich domain with the intensity of F8BT emission that was measured simultaneously. Figure 3b similarly compares a cross-section of the topography across a PFO/F8BT interface with the intensity of PFO emission. It can be seen that there is a bright band of PFO emission that is approximately 300 nm in width located at the boundary of the PFO-rich phase. This emission is approximately 1.6 times brighter than the PFO emission detected at the centre of the PFO-rich domain. This increase in PFO intensity appears to be well correlated with a gradual reduction in the F8BT emission intensity that also occurs towards the PFO/F8BT boundary. It is clear that in images in Fig. 2b,d,f that the probe follows a very similar path as it scans the film surface. However, the optical image generated seems to be highly dependent on the wavelength of light that is detected, which indicates that the SNOM image derives from the optical properties of the film rather than being dependent on changes in probe-surface separation³⁰.

To determine the homogeneity of the blend normal to the surface, we have used ${}^3\text{He}$ NRA. This technique can be used to determine the depth-dependent composition of deuterium in a thin film^{31,32}.

By deuterium-labelling PFO (d-PFO), we have been able to determine the depth-dependent composition of d-PFO in a 1:1 d-PFO/F8BT blend film. Control SFM scans demonstrated that such blends had a very similar surface structure to non-deuterated blends, giving us confidence that the results of such analysis can be reasonably compared with the results of our SNOM measurements. Figure 4 shows the volume fraction of d-PFO as a function of depth normal to the surface of the film. Once we account for the finite resolution of the technique, we find that there is a 10-nm-thick layer at the film surface that is enriched in d-PFO, with the top 5 nm of the film being composed of almost 'pure' d-PFO. Deeper into the film, the relative fractions of d-PFO to F8BT are approximately equal. As the NRA measurement has no sensitivity to lateral surface structure, we conclude that in 1:1 PFO/F8BT blends, an enriched PFO surface layer runs continuously over both the PFO- and F8BT-rich domains. Surface enrichment layers of ~15 nm in thickness have also been observed in blends of other polyfluorenes using SFM, and have been shown to improve the performance of polymer-blend optoelectronic devices^{8,14}. Injection of electrons into the surface of this film, however, may not be a particularly efficient process due to the problems associated with electron trapping¹⁸ in PFO.

To characterize the surface structure of the blend in more detail, we have used an SFM operating in tapping mode. Figure 5 shows an SFM image recorded in the centre of a PFO-rich domain. It can be seen in both the topographic image (Fig. 5a) and the phase-contrast image (Fig. 5b), that the surface of the film is characterized by fibrils of approximately 10 nm in width. The NRA indicates that the blend surface is almost pure PFO, indicating that the fibrils we observe result from the self-organization or association of PFO molecules. Note, however, that such fibril-like structures are not observed over the whole film surface; over the F8BT-rich domains we typically observe an amorphous distribution of polymer, indicating that the formation of surface structure appears to be highly dependent on the composition of the underlying phase. We speculate that each fibril may be a bundle of partially crystallized PFO molecules, with the media between the fibrils being composed of amorphous PFO and perhaps residual amounts of F8BT. The partial crystallization of the surface layer is consistent with a PFO-rich layer being located at the surface, because such surface crystallization during spin-coating may well contribute to the thermodynamic driving-forces which favour the expulsion of the F8BT molecules from the surface to the subsurface layers. The assignment of partial crystallinity is consistent with the fact that PFO is a rigid-rod polymer, which can be driven into a crystalline form by appropriate thermal cycling³³. Other SFM measurements on polyindenofluorenes (which are also believed to undergo π -stacking)³⁴ similarly identify fibril-like structures, however, such fibrils are not observed on the surface of freshly spun PFO films³⁵.

We thus identify a hierarchy of structure on a number of different length-scales: micrometre-sized phase separation, a bright band of residual PFO emission that occurs on a length scale of a few hundred nanometres, and a partially crystallized surface layer of PFO having a thickness of ~10 nm. These observations allow us to gain insight into the residual PFO emission that is emitted from the blend. It is probable that the majority of such emission comes from the surface-rich layer of PFO. From the absorption coefficient of PFO, we estimate that ~30% of the incident laser-light is directly absorbed by this surface layer. There must, however, be a degree of energy transfer between PFO and F8BT within this surface layer, because the residual PFO emission comprises only 5% of the total emission. This energy transfer may occur to F8BT molecules that are present at low concentration in the surface layer. However, excitons may also transfer from the surface to the 'bulk' where the local concentration of F8BT molecules is much greater. Diffusion and transfer from the surface layer to the 'bulk' is likely to be a rapid and efficient process, because the thickness of the PFO surface layer is commensurate with the Förster transfer radius for this system²⁹ and the exciton diffusion length for excitons¹³ in PFO (both estimated to be ~5 nm).

The presence of a continuous PFO surface layer explains why we observe PFO emission from the F8BT-rich domains. It also accounts for the fact that such PFO emission appears to be relatively diffuse compared with the structured F8BT emission. Note, however, the relative weakness of the residual PFO emission observed from the F8BT-rich domains cannot simply be accounted for by optical absorption of the PFO emission in the subsurface F8BT layer. It is more likely that the large concentration of F8BT molecules situated beneath the PFO surface layer results in relatively enhanced energy transfer from the surface to the 'bulk'. There is one feature of the residual PFO emission that defies ready explanation; that is the relatively bright band of PFO emission that is observed at the boundary between the F8BT- and PFO-rich domains. This could occur from an increase in the thickness of the PFO surface layer towards the interface. Although we cannot conclusively reject this hypothesis, we do not observe any clear changes in the surface morphology that consistently coincide with changes in the fluorescence intensity. It is possible that this enhanced residual emission does not originate from the surface, but instead comes from regions deeper in the film. This could also account for its relative diffuseness, because if it were no longer being generated in the optical near-field of the tip (within some 10 nm or so of the surface), high optical resolution could no longer be achieved.

We propose that such enhanced residual emission may result from a relative depletion of the concentration of F8BT acceptor molecules at the edge of PFO-rich domains. This depletion could arise naturally from diffusion of the F8BT molecules that remain in a PFO-rich solution immediately after the F8BT-rich domains have vitrified. This diffusion process across the interface between the solution and the F8BT rich domains may be driven by phase separation, and therefore the structures we observe represent a snapshot of the polymer blend approaching (but not reaching) equilibrium. Further work will be necessary to confirm the presence of such a depleted region, however it is clear that the structure or composition of the interface is different from what is found in either of the two individual phases.

Such types of interface structures are unlikely to be restricted to this particular combination of polymers. Rather, they may occur quite generally in other blends of phase-separated conjugated polymers. SFM measurements on other F8BT-based polyfluorene blends (which are used in both PV and LED devices^{11,14,15}) reveal surface structure that in many cases appears to be very similar to that observed here¹⁵. It is therefore probable that the interface structure that we have observed here may also be present in other polyfluorene blends and may play an important role in PVs and LEDs by acting as heterojunctions where charge separation or exciton generation occurs. If it proves possible to control the structure of such interfaces by, for example, controlling the film-casting protocol, it will help to determine their role in polymer-blend devices and may provide a powerful method to optimize device performance.

METHODS

PFO/F8BT films were prepared by dissolving the two polymers in a toluene solution to a final concentration of 1% by weight. The solution was then spin-coated onto a glass slide to give a film having an average thickness of 60 nm. For the NRA measurements, the PFO was deuterium labelled by substituting the hydrogen atoms on the octyl side-groups (on alternate fluorene monomers) with deuterium.

Far-field absorption measurements of thin films were made using a UNICAM UV500 spectrometer. To measure far-field fluorescence, blend films were excited using the 326 nm line of a Spectra-Physics 2020 Argon-Ion laser. Fluorescence spectra were measured using an Oriel Instruments Spectrograph (0.25 m) coupled to an Andor Technology CCD camera.

Our near-field optical microscope system is based on a Veeco Aurora SNOM. We use fibre probes supplied by Jasco International (Tokyo). The probes have an aperture that is between 60 and 80 nm in diameter and have an optical throughput of 1.5% at 360 nm. The probes have negligible inherent fluorescence, making them ideal for sensitive SNOM spectroscopy of ultraviolet-absorbing materials. Excitation of the blend films was made through the probe using the 362-nm line from an argon-ion laser (as above). The laser was first spectrally filtered using an interference filter to remove the laser plasma lines. A 0.25 numerical aperture microscope objective located beneath the sample collected the transmitted fluorescence and laser light and imaged it through a series of dielectric filters (Andover Corporation, filters 400, 450, 500 and 550 FL07) onto a high-gain, low-noise photomultiplier (PMT)

working in current-mode (Electron Tubes, model 9124). The probe-sample distance was controlled by shear-force feedback with the probe mounted on a quartz crystal tuning fork (Veeco Accutune, 1641-00). All imaging was done at room temperature and in air. We did not detect any significant photo-oxidation of the polymer film (as would be seen by a drop in the photoluminescence intensity) during the course of a scan. The images presented are representative of a large number of repeat scans made using a series of different SNOM probes at different points on the film surface.

For ultraviolet-transmission experiments, a series of dielectric-filters (as above) were placed in front of the PMT to cut all fluorescence in the range 400 to 700 nm. The remaining ultraviolet laser light was then imaged onto the PMT photocathode. When imaging fluorescence, an ultraviolet rejection filter (of optical density 4 at 360 nm) was placed in front of the PMT to remove the laser excitation light, and the dielectric filter combination was varied to select the wavelength interval of interest: one filter combination rejected all light above 460 nm, allowing only the PFO emission to be detected. Otherwise a different filter combination was used to reject all light below 490 nm, allowing only F8BT emission to be detected. To confirm that the SNOM images are consistent with our far-field spectroscopic measurements, the average intensity of F8BT (I_{F8BT}) and PFO (I_{PFO}) emission was determined from the images in Fig. 2d and f respectively. After correction for the wavelength-dependent efficiency of the PMT detector and the power of the laser, we find that $I_{\text{PFO}}/I_{\text{F8BT}} \approx 0.10$, a value in close accord with far-field fluorescence measurements in which $I_{\text{PFO}}/I_{\text{F8BT}} \approx 0.05$.

The laser power focused into the SNOM fibre was typically between 0.25 and 1 mW, equivalent to a power density at the film surface of $\sim 2 \text{ GW m}^{-2}$. At this power density we do not anticipate photobleaching of the polymer ground state. It can be shown that a very thin layer of molecules having an absorption cross-section of σ , exposed to a photon flux n , will absorb a photon on average once every $(\sigma n)^{-1}$ seconds. Using a value of the singlet absorption cross-section for PFO as¹⁷ $\sigma = 1.4 \times 10^{-20} \text{ m}^2$, and taking n to be $4 \times 10^{27} \text{ s}^{-1} \text{ m}^{-2}$, we calculate that a PFO molecule sitting on the surface of the film (exposed to the maximum photon flux from the SNOM tip) will absorb a photon every $\sim 20 \text{ ns}$. This time is significantly longer than the spontaneous emission lifetime of PFO (430 ps, ref. 17), thus it appears that most of the PFO molecules at any one time are in the ground state. The same conclusion also applies to F8BT molecules, which have a smaller absorption cross-section than PFO at the laser wavelength.

Ion-beam experiments were performed using a National Electronics Corporation 5SDH series Pelletron accelerator facility at the University of Durham. $^3\text{He}^+$ ions were accelerated to 700 keV before being incident on the polymer film at a glancing angle of 6° . The $^3\text{He}^+$ exposure delivered to the sample during any one measurement was limited to $5 \mu\text{C}$. The depth profile of PFO determined from consecutive scans recorded from the same position on the sample surface were very similar, indicating that the exposure dose used was not sufficient to cause significant damage to the blend film.

Received 6 December 2002; accepted 15 July 2003; published 17 August 2003.

References

1. Friend, R. H. *et al.* Electroluminescence in conjugated polymers. *Nature* **397**, 121–128 (1999).
2. Bernius, M. T., Inbasekaran, M., O'Brien, J. & Wu, W. Progress with light-emitting polymers. *Adv. Mater.* **12**, 1737–1750 (2000).
3. Wilkinson, C. I. *et al.* Enhanced performance of pulse driven small area polyfluorene light emitting diodes. *Appl. Phys. Lett.* **79**, 171–173 (2001).
4. Morgado, J., Friend, R. H. & Cacialli, F. Improved efficiency of light-emitting diodes based on polyfluorene blends upon insertion of a poly(p-phenylene vinylene) electron-confinement layer. *Appl. Phys. Lett.* **80**, 2436–2438 (2002).
5. Halls, J. J. M. *et al.* Efficient photodiodes from interpenetrating polymer networks. *Nature* **376**, 498–500 (1995).
6. van Hutten, P. F., Krasnikov, V. V. & Hadziioannou, G. in *Conjugated Polymer and Molecular Interfaces* (eds Salaneck, W., Seki, K., Kahn, A. & Pireaux, J. J.) 113–142 (Marcel Dekker, New York, 2001).
7. Chen, L. *et al.* Excitation transfer in polymer photodiodes for enhanced quantum efficiency. *Adv. Mater.* **12**, 1110–1114 (2000).
8. Arias, A. C. *et al.* Vertically segregated polymer-blend photovoltaic thin-film structures through surface-mediated solution processing. *Appl. Phys. Lett.* **80**, 1695–1697 (2002).
9. Campbell, A. J. *et al.* in *Proceedings of SPIE 2002 4464* (ed. Kafafi, Z. H.) 211–222 (SPIE, Washington, 2002).
10. Geoghegan, M. & Krausch, G. Wetting at polymer surfaces and interfaces. *Prog. Polym. Sci.* **28**, 261–302 (2003).
11. Halls, J. J. M. *et al.* Photodiodes based on polyfluorene composites: influence of morphology. *Adv. Mater.* **12**, 498–502 (2000).
12. Halls, J. J. M., Pichler, K., Friend, R. H., Moratti, S. C. & Holmes, A. B. Exciton diffusion and dissociation in a poly(p-phenylenevinylene) / C-60 heterojunction photovoltaic cell. *Appl. Phys. Lett.* **68**, 3120–3122 (1996).
13. Stoessel, M. *et al.* Cathode-induced luminescence quenching in polyfluorene. *J. Appl. Phys.* **87**, 4467–4475 (2000).
14. Snaith, H. J., Arias, A. C., Morteani, A. C., Silva, C. & Friend, R. H. Charge generation kinetics and transport mechanisms in blended polyfluorene photovoltaic devices. *Nano Lett.* **2**, 1353–1357 (2002).
15. Moons, E. Conjugated polymer blends: linking film morphology to performance of light emitting diodes and photodiodes. *J. Phys. Condens. Matter* **14**, 12235–12260 (2002).
16. Corcoran, N., Arias, A. C., Kim, J. S., MacKenzie, J. D. & Friend, R. H. Increased efficiency in vertically segregated thin-film conjugated polymer blends for light-emitting-diodes. *Appl. Phys. Lett.* **82**, 299–301 (2003).
17. Ariu, M. *et al.* The effect of morphology on the temperature-dependent photoluminescence quantum efficiency of the conjugated polymer poly(9,9-dioctylfluorene). *J. Phys. Condens. Matter* **14**, 9975–9986 (2002).
18. Redecker, M., Bradley, D. D. C., Inbasekaran, M. & Woo, E. P. Nondispersive hole transport in an electroluminescent polyfluorene. *Appl. Phys. Lett.* **73**, 1565–1567 (1998).
19. Herguth, P., Jiang, X., Liu, M. S. & Jen, A. K. Y. Highly efficient fluorene- and benzothiadiazole-based conjugated copolymers for polymer light-emitting diodes. *Macromolecules* **35**, 6094–6100 (2002).
20. Campbell, A. J., Bradley, D. D. C. & Antoniadis, H. Dispersive electron transport in an electroluminescent polyfluorene copolymer measured by the current integration time-of-flight method. *Appl. Phys. Lett.* **79**, 2133–2135 (2001).
21. Buckley, A. R. *et al.* Energy transfer dynamics in polyfluorene-based polymer blends. *Chem. Phys. Lett.* **339** 331–336 (2001).
22. Wei, P. K., Hsu, J. H. & Fann, W. S. Study of conjugated polymer blend films by a near field scanning optical microscopy. *Synth. Met.* **102**, 1209–1210 (1999).
23. DeAro, J. A., Weston, K. D., Buratto, S. K. & Lemmer, U. Mesoscale optical properties of conjugated polymers probed by near-field scanning optical microscopy. *Chem. Phys. Lett.* **277**, 532–538 (1997).
24. Chappell, J. & Lidzey, D. G. Phase-separation in polyfluorene-polymethylmethacrylate blends studied using UV near-field microscopy. *J. Microsc.* **209**, 188–193 (2003).
25. Webster, S., Smith, D. A., Batchelder, D. N., Lidzey, D. G. & Bradley, D. D. C. Application of fluorescence scanning near-field optical microscopy to the study of phase-separated conjugated polymers. *Ultramicroscopy* **71**, 275–279 (1998).
26. Stevenson, R., Granström, M. & Richards, D. Fluorescence scanning near-field optical microscopy of conjugated polymer blends. *Appl. Phys. Lett.* **75**, 1574–1576 (1999).
27. Stevenson, R. *et al.* Ultraviolet-visible near-field microscopy of phase-separated blends of polyfluorene-based conjugated semiconductors. *Appl. Phys. Lett.* **79**, 833–835 (2001).
28. Stevenson, R. *et al.* Fluorescence scanning near-field optical microscopy of polyfluorene composites. *J. Microsc.* **202**, 433–438 (2001).
29. Morgado, J., Moons, E., Friend, R. H. & Cacialli, F. De-mixing of polyfluorene-based blends by contact with acetone: electro- and photo-luminescent probes. *Adv. Mater.* **13**, 810–814 (2001).
30. Hecht, B., Bielefeldt, H., Inouye, Y., Pohl, D. W. & Novotny, L. Facts and artefacts in near-field optical microscopy. *J. Appl. Phys.* **81**, 2492–2498 (1997).
31. Payne, R. S., Clough, A. S., Murphy, P. & Mills, P. J. Use of the $d(^3\text{He}, p)^4\text{He}$ reaction to study polymer diffusion in polymer melts. *Nucl. Instrum. Meth. B* **42**, 130–134 (1989).
32. Geoghegan, M. in *Polymer Surfaces and Interfaces III* (eds Richards, R. W. & Peace, S. K.) 43–73 (Wiley, Chichester, 1999).
33. Grell, M., Bradley, D. D. C., Inbasekaran, M. & Woo, E. P. A glass-forming conjugated main-chain liquid crystal polymer for polarized electroluminescence applications. *Adv. Mater.* **9**, 798–803 (1997).
34. Grimsdale, A. C. *et al.* Correlation between molecular structure, microscopic morphology and optical properties of poly(tetraalkylindeno[1,2-b]fluorene)s. *Adv. Funct. Mater.* **12**, 729–733 (2002).
35. Ariu, M. *et al.* A study of the different structural phases of the polymer poly(9,9-dioctylfluorene) using Raman spectroscopy. *Synth. Met.* **116**, 217–221 (2001).

Acknowledgements

We thank the UK Engineering and Physical Sciences Research Council for support of this research through grants GR/R26658/01 and GR/R10479/01 and for the provision of funding for D.G.L. and J.C. We also thank Franco Cacialli and Simon Martin for useful comments and discussions. Correspondence and requests for materials should be addressed to D.G.L.

Competing financial interests

The authors declare that they have no competing financial interests.